

SoftDropConnect (SDC) – Effective and Efficient Quantification of the Network Uncertainty in Deep MR Image Analysis

Qing Lyu¹, Christopher T. Whitlow^{3-10,*}, and Ge Wang^{1-2,*}

¹Department of Biomedical Engineering, Rensselaer Polytechnic Institute, Troy, NY, USA

²Biomedical Imaging Center, Center for Biotechnology and Interdisciplinary Studies, Rensselaer Polytechnic Institute, Troy, NY, USA

³Comprehensive Cancer Center, Wake Forest School of Medicine, Winston-Salem, NC, USA

⁴Brain Tumor Center of Excellence, Wake Forest School of Medicine, Winston-Salem, NC, USA

⁵Radiology Informatics & Image Processing Laboratory, Wake Forest School of Medicine, Winston-Salem, NC, USA

⁶Department of Radiation Oncology, Wake Forest School of Medicine, Winston-Salem, NC, USA

⁷Department of Radiology, Wake Forest School of Medicine, Winston-Salem, NC, USA

⁸Department of Neurosurgery, Wake Forest School of Medicine, Winston-Salem, NC, USA

⁹Department of Neurology, Wake Forest School of Medicine, Winston-Salem, NC, USA

¹⁰Department of Biomedical Engineering, Wake Forest School of Medicine, Winston-Salem, NC, USA

*Corresponding author

ABSTRACT

Recently, deep learning has achieved remarkable successes in medical image analysis. Although deep neural networks generate clinically important predictions, they have inherent uncertainty. Such uncertainty is a major barrier to report these predictions with confidence. In this paper, we propose a novel yet simple Bayesian inference approach called SoftDropConnect (SDC) to quantify the network uncertainty in medical imaging tasks with gliomas segmentation and metastases classification as initial examples. Our key idea is that during training and testing SDC modulates network parameters continuously so as to allow affected information processing channels still in operation, instead of disabling them as Dropout or DropConnet does. When compared with three popular Bayesian inference methods including Bayes By Backprop, Dropout, and DropConnect, our SDC method (SDC-W after optimization) outperforms the three competing methods with a substantial margin. Quantitatively, our proposed method generates results with substantially improved prediction accuracy (by 10.0%, 5.4% and 3.7% respectively for segmentation in terms of dice score; by 11.7%, 3.9%, 8.7% on classification in terms of test accuracy) and greatly reduced uncertainty in terms of mutual information (by 64%, 33% and 70% on segmentation; 98%, 88%, and 88% on classification). Our approach promises to deliver better diagnostic performance and make medical AI imaging more explainable and trustworthy.

Introduction

Over the past decade, various deep neural networks (DNNs) have been developed and revolutionized our capabilities in different domains. In the field of medical image analysis, DNNs can now generate far better results than conventional feature-based methods in many applications such as nodule detection¹, tumor segmentation², and cancer staging³. In these cases, neural networks were mostly trained to produce point estimates by optimizing network parameters to minimize objective functions. Normally, after the training stage all network parameters are fixed and kept unchanged in the inference stage. As a result, for the same input the network will produce the same output. For these neural networks, it is inevitable to generate both accurate and inaccurate predictions, but there is no estimation on the reliability of these predictions. This limitation is major for the deployment of deep learning methods in healthcare-critical real-world applications⁴.

For tumor imaging⁵⁻⁹, estimating the network uncertainty allows clinicians to reject network predictions of high uncertainty and use additional methods such as biopsy and bio-markers to effectively mitigate false predictions. Generally speaking, there are two types of network uncertainties: model or epistemic uncertainty and data or aleatoric uncertainty. Epistemic uncertainty accounts for fuzziness in the model parameters from data insufficiency and model mismatching, while aleatoric uncertainty measures inherently data noise¹⁰. Properly measuring uncertainty is of critical importance. Researchers tried to use the softmax in the final layer to infer the confidence of classification predictions, and found that networks could generate inaccurate predictions with high softmax-type pseudo possibility. In this case, the softmax probability only reflects the possibility of a given class relative to other classes on a specific input and does not show an overall confidence^{11,12}.

To better estimate the network uncertainty, many methods were proposed in recent years. Based on the number and the nature of the used DNNs, we can classify them into the single deterministic^{13–15}, Bayesian^{11,16,17}, ensemble^{18–20}, and test-time augmentation categories^{21–24}. Among these classes, variational Bayesian inference is a commonly used approach. Different from deterministic DNNs, parameters of a Bayesian neural network (BNN) are not fixed but described with a posterior possibility distribution²⁵. Since the estimation of such a posterior possibility distribution is often intractable, researchers proposed variational inference to approximate the posterior possibility distribution as a series of simpler variational distributions²⁶. To optimize BNNs, Bayes by Backprop (BBB)¹⁷, local reparameterization²⁷, and multiplicative normalising flows²⁸ are commonly used training methods. Mathematically equivalent approximation to BNNs, Monte Carlo DropOut is another popular method to estimate the network uncertainty, which performs dropout on every network layer in both training and inference stages¹⁶. As a generalization to Dropout, DropConnect was recently proposed to replace Dropout, which is called Monte Carlo DropConnect¹¹.

In this paper, we modify DropConnet so that weights in drop masks are modulated according to a continuous uniform distribution instead of a discrete Bernoulli distribution, extending the DropConnect method to a generalized version, which is referred to as SoftDropConnect (SDC). Then, we investigate the performance of SDC using Monte Carlo methods for network uncertainty estimation in medical applications by comparing our method with other variational Bayesian inference methods. Our main contributions in this paper are as follows:

1. SDC is designed as a generalized version of DropConnect by sampling drop weights from a uniform distribution.
2. SDC is applied to estimate the network uncertainty. In comparison with other variational Bayesian inference methods, the utilities and merits of SDC are demonstrated.
3. Two variants of SDC, SDC-Strong and SDC-Weak, are further proposed to estimate the network uncertainty. Our results show that SDC-Weak outperforms SDC and SDC-Strong with higher accuracy and lower uncertainty.
4. In two applications for gliomas segmentation and metastases classification respectively, our approach is effective to improve prediction accuracy and avoid false predictions, showing a great potential of this technique in future clinical applications.

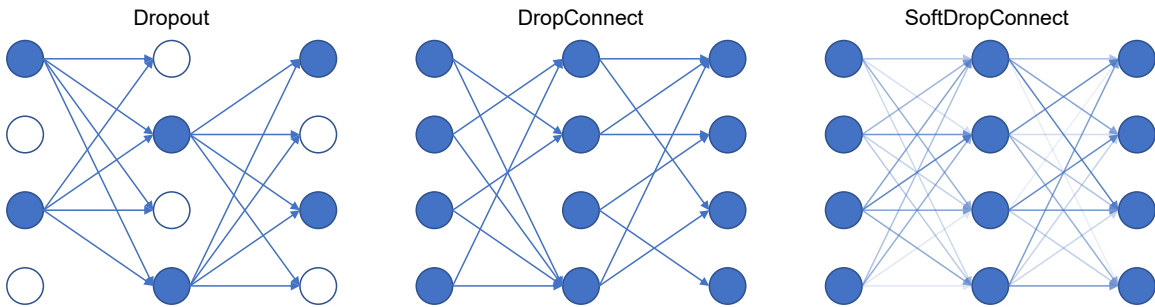


Figure 1. Comparison of Dropout (left), DropConnect (middle), and SoftDropConnect (right). For Dropout and DropConnect, connection drop mask weights are either ones (in blue) or zeros (in white). For Soft DropConnect, connection drop mask weights are continuous; for example, between one and zero.

Results

In this study, to estimate the network uncertainty, we propose a SoftDropConnect approach called SDC by replacing drop weights from a Bernoulli distribution into that from a continuous uniform distribution such as $\sim U(0, 1)$. As two variants, we limit the drop weight distribution ranges to have SDC-Strong or SDC-S (drop weights $\sim U(0, 0.5)$) and SDC-Weak or SDC-W (drop weights $\sim U(0.5, 1)$). To show the merits of our approach, we compare the three versions (SDC, SDC-S, SDC-W) of our approach with popular variational Bayesian inference methods: Bayes by Backprop¹⁷ (BBB), Monte Carlo DropOut¹⁶, and Monte Carlo DropConnect¹¹. For simplicity, we call Monte Carlo DropOut and Monte Carlo DropConnect as Dropout and DropConnect respectively in this paper. Experiments are conducted on three datasets: the MNIST dataset for digit recognition, the BraTS dataset for gliomas segmentation, and our in-house brain metastases dataset for tumor origin site classification.

Datasets

As a starting point, MNIST dataset²⁹ was used for digit recognition. In this study, 50,000 images were used for training, and 10,000 images for validation and testing. Then, BraTS 2021 dataset³⁰ was used for gliomas segmentation. In the provided training dataset, there are 1,251 cases, each of which contains human-labeled segmentation ground truth and MR images in four modalities: T1-weighted, T1 contrast enhancing (T1CE), T2-weighted, and T2 Fluid Attenuated Inversion Recovery (FLAIR). We used the first 400 cases for training, the next 100 cases for validation, and the last 50 cases for testing. Finally, our own brain metastases dataset was used for tumor origin site classification. This dataset was collected at Wake Forest School of Medicine from 2000 to 2021. Detailed information and data pre-processing steps were described in³¹. As shown in Fig 3a, in this study we used 1,200 cases for training, 150 cases for validation ,and 232 cases for testing.

Uncertain estimation on the MNIST dataset for digit recognition

The MNIST dataset is widely used as a toy example in machine learning research. In this study, we first used MNIST to demonstrate the effectiveness of our proposed methods for uncertainty estimation. Based on^{4,32}, mutual information was adopted to reflect epistemic uncertainty. In addition to mutual information, we adopted the prediction class count and the prediction popular voting class softmax possibility count to evaluate uncertain estimation.

We compared six variational Bayesian inference methods on the MNIST dataset. As shown in Fig. 2a-c, SDC outperforms BBB, Dropout, and DropConnect with higher accuracy and lower mutual information. Among our proposed SDC, SDC-S, and SDC-W methods, SDC-W has the highest accuracy and the lowest mutual information. Quantitatively, SDC-W can achieve the lowest mutal information among all the methods. When setting the leave out rate $p = 0.5$, compared with BBB, Dropout, DropConnect, SDC, and SDC-S methods, SDC-W greatly lowered mutual information by 76%, 82%, 69%, 37%, and 50%, respectively. In terms of the test prediction accuracy, SDC-W increased accuracy by 0.47%, 0.47%, 0.59%, 0.09%, and 0.23%, respectively.

One testing case is demonstrated in Fig. 2d. It can be observed that almost every SDC-W prediction is correct, and these predictions are with very high softmax possibilities. Moreover, the SDC-W prediction is with the lowest mutual information value when compared with the other methods. All these results demonstrate that SDC-W is rather confident in its prediction. In contrast, the other results are with more uncertainty. For example, most Dropout predictions are counted in the bin for digit 3, showing false predictions. It is seen in the prediction class softmax possibility chart that only about 40% of all predictions are counted in the last bin with a very high softmax possibility. Compared with SDC-W, the neural network is much less confident about DropConnect results. More examples are presented in Supplementary Fig. 1.

Uncertain estimation on the BraTS dataset for gliomas segmentation

To demonstrate the relevance of uncertainty estimation to medical applications, we selected the BraTS dataset for gliomas segmentation. We used 1) dice scores of whole tumor, tumor core, and enhanced tumor, 2) pixel-wise mutual information, 3) absolute error between mean prediction and ground truth, and 4) standard deviation to reflect the segmentation uncertainty.

Similar to our results on the MNIST dataset, it is observed in Fig. 3a and b that the SDC results are better than the BBB, Dropout, and DropConnect counterparts in terms of validation accuracy and whole tumor dice score. Among SDC, SDC-S, and SDC-W results, the SDC-W results achieved the highest validation accuracy and whole tumor dice score. As far as the effect of leave out rate p on the network performance is concerned, it is shown in Fig. 3b that whole tumor dice scores of SDC and SDC-W were decreased relatively less when the leave out rate p was increased from 0.05 to 0.5. Table 1 shows dice scores of whole tumor, tumor core, and enhanced tumor segmentation results. Again, SDC-W produced the best results in segmenting all three gliomas components. To quantify uncertainty, we adopted the average mutual information over all pixels. Under the setting of $p = 0.05$, compared with BBB, Dropout, DropConnect, SDC, and SDC-S, SDC-W significantly lowered mutual information by 64%, 33%, 70%, 42%, and 49%, respectively. For the whole tumor dice score, SDC-W presented results with the improvement by 10.0%, 5.4%, 3.7%, 0.8%, and 3.7%, respectively.

Fig. 3c represents an example of segmentation uncertain estimation. In terms of mean prediction results in the second row, consensus predictions will lead to clearer edges and shapes, resulting in less network uncertainty. In terms of prediction standard deviations in the fourth row, less highlighted areas demonstrates predictions more likely to be the same, suggesting less uncertainty. In the bottom row of pixel-wise mutual information, larger mutual information values reflect higher network uncertainty. Among all the six methods, SDC-W produced the best voting results. For example, the white spot pointed by the blue arrow can be clearly segmented in SDC-W's most popular voting results in the first row. When mean prediction, prediction standard deviation and mutual information were used to evaluate network uncertainty, SDC-W also demonstrated results with the least uncertainty. Supplementary Figs. 2 and 3 contain more results on the effect of the leave out rate p . Increasing the leave out rate p seemed increasing network uncertainty while decreasing segmentation accuracy.

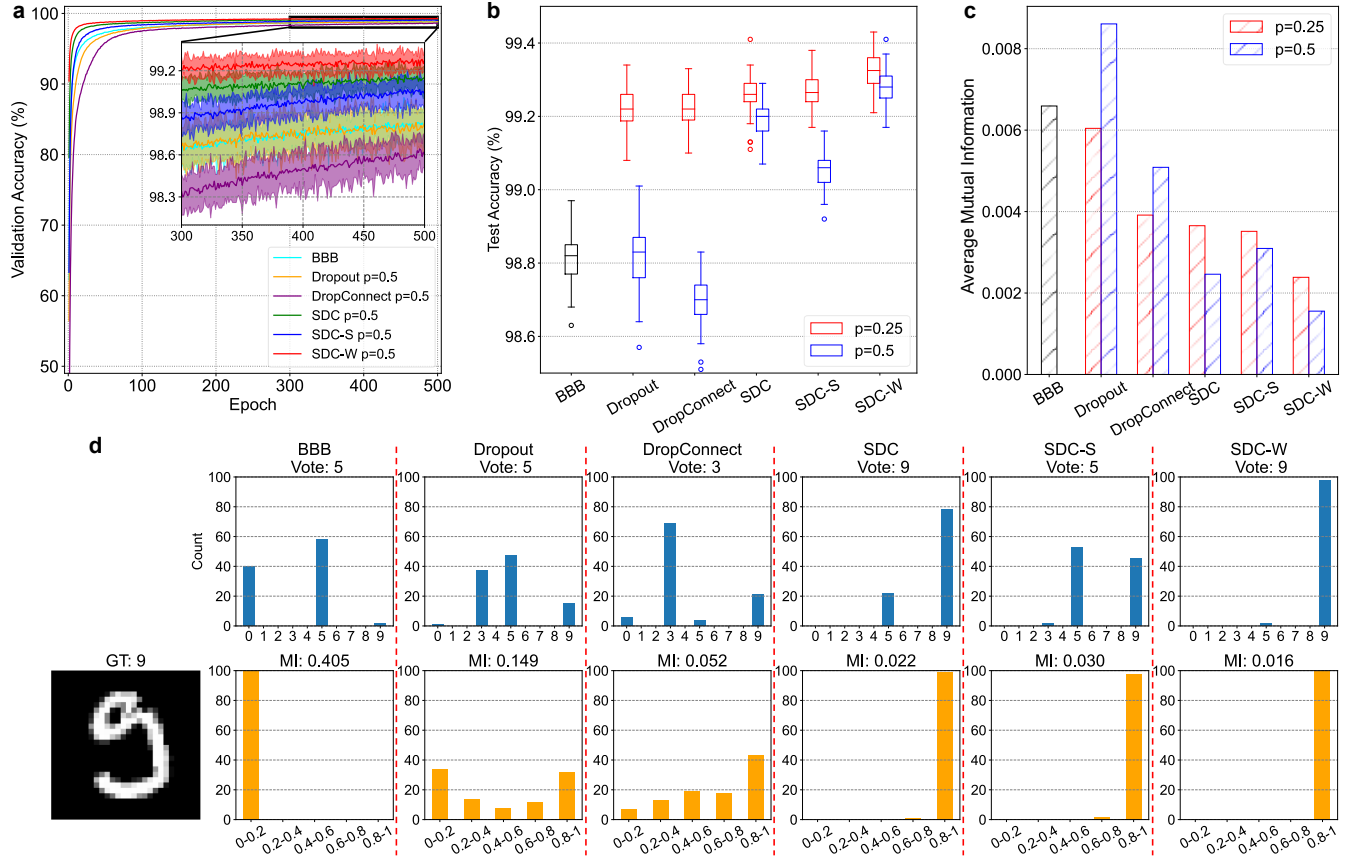


Figure 2. Uncertainty estimation results on the MNIST dataset for digit recognition. a) The validation accuracy during the training process. Solid lines show average accuracy and bands reflect the min-max range, b) the box plot of accuracy results on test data from different variational Bayesian inference methods with 0.25 or 0.5 leave out rates respectively, c) the bar chart of average mutual information on test data, and d) a testing case with a leave out rate $p = 0.5$. In d), The top row gives the each class prediction counts, and the subplot title shows the most popular prediction class voting result; The bottom row lists softmax probability counts corresponding to the popular voting class, and the subplot title is the mutual information value.

Uncertain estimation on the brain metastases dataset for tumor origin site classification

Finally, we used our own dataset to perform brain metastases origin site classification with network uncertainty estimation. Followed our previous work³¹, we upgraded the previously proposed classification framework with a capability of estimating the network uncertainty. Similar to what we did in the MNIST digit recognition task, here we also adopted the prediction class count, prediction popular voting class softmax possibility count, and mutual information to evaluate the network uncertainty.

Table 2 compares the selected methods with different leave out rates. It can be found that mutual information increases with a larger leave out rate p , indicating that an ascending leave out rate p will result in larger network uncertainty. SDC yielded a lower mutual information measure than BBB, Dropout, and DropConnect, and SDC-W produced the lowest mutual information. In terms of setting the leave out rate $p = 0.05$, compared with BBB, Dropout, DropConnect, SDC, and SDC-S methods, SDC-W greatly lowered mutual information 98%, 88%, 88%, 56%, and 74%, respectively. In Fig. 4b-c, SDC-W gave the best classification results with the highest prediction accuracies in the validation and test phases. Compared with other methods with $p = 0.05$, SDC-W substantially improved prediction accuracy by 11.7%, 3.9%, 8.7%, 0.6%, and 3.4%, respectively. Fig. 4d demonstrates that the use of the network uncertainty helped avoid false predictions. The average softmax possibility of prediction popular voting class was used as the uncertainty threshold. When we gradually increase the uncertainty threshold, a growing number of prediction results with high uncertainty estimation will be rejected, meaning that a less number of predictions could be made. On the other hand, for the predictions the network makes, the accuracy should be increasingly higher.

Fig. 4e represents the average prediction class counts and the average softmax possibility counts of prediction popular voting class. A higher average prediction class count indicates that prediction results tends to be more consistent in the test phase. When comparing all the six methods, it is clearly that SDC-W gives the highest average prediction class counts. In

Table 1. Dice Score Comparison on the BraTS dataset for gliomas segmentation (MEAN \pm SD), where “MEAN” and “SD” represent the mean and standard deviation respectively.

		Whole Tumor	Tumor Core	Enhanced Tumor
BBB	-	0.803 \pm 0.013	0.807 \pm 0.021	0.754 \pm 0.017
Dropout	p=0.05	0.839 \pm 0.011	0.823 \pm 0.009	0.763 \pm 0.006
	p=0.25	0.801 \pm 0.014	0.797 \pm 0.014	0.753 \pm 0.006
	p=0.50	0.718 \pm 0.016	0.710 \pm 0.016	0.729 \pm 0.010
DropConnect	p=0.05	0.852 \pm 0.018	0.818 \pm 0.017	0.755 \pm 0.017
	p=0.25	0.812 \pm 0.032	0.767 \pm 0.030	0.711 \pm 0.039
	p=0.50	0.698 \pm 0.037	0.682 \pm 0.046	0.610 \pm 0.058
SDC	p=0.05	0.876 \pm 0.013	0.833 \pm 0.020	0.761 \pm 0.016
	p=0.25	0.860 \pm 0.020	0.819 \pm 0.024	0.732 \pm 0.033
	p=0.50	0.815 \pm 0.033	0.731 \pm 0.027	0.716 \pm 0.037
SDC-S	p=0.05	0.852 \pm 0.019	0.824 \pm 0.021	0.748 \pm 0.017
	p=0.25	0.826 \pm 0.027	0.790 \pm 0.030	0.708 \pm 0.024
	p=0.50	0.808 \pm 0.032	0.686 \pm 0.046	0.637 \pm 0.059
SDC-W	p=0.05	0.884 \pm 0.012	0.845 \pm 0.008	0.771 \pm 0.014
	p=0.25	0.874 \pm 0.013	0.810 \pm 0.024	0.758 \pm 0.023
	p=0.50	0.848 \pm 0.020	0.802 \pm 0.018	0.753 \pm 0.018

addition to the average prediction class count, we also considered the average softmax possibility counts of prediction class to evaluate the network uncertainty. The network becomes more confident about its predictions when more counts are in the right-most bin with the highest softmax possibility. Compared with BBB and Dropout, DropConnect, SDC, SDC-S and SDC-W generated more counts in those bins with a higher softmax possibility. Among all the methods, SDC-W seems the best, delivering the highest average prediction class counts and the most counts in relatively certain bins.

Table 2. Mutual Information Comparison on the Brain Metastases dataset for tumor origin site segmentation (MEAN \pm SD), where “MEAN” and “SD” represent the mean and standard deviation respectively.

		Mutual Information
BBB	-	0.048 \pm 0.026
Dropout	p=0.05	0.007 \pm 0.005
	p=0.25	0.012 \pm 0.006
	p=0.50	0.018 \pm 0.003
DropConnect	p=0.05	0.007 \pm 0.004
	p=0.25	0.014 \pm 0.003
	p=0.50	0.009 \pm 0.002
SDC	p=0.05	0.002 \pm 0.001
	p=0.25	0.007 \pm 0.004
	p=0.50	0.010 \pm 0.003
SDC-S	p=0.05	0.003 \pm 0.002
	p=0.25	0.008 \pm 0.005
	p=0.50	0.015 \pm 0.003
SDC-W	p=0.05	0.001 \pm 0.001
	p=0.25	0.003 \pm 0.003
	p=0.50	0.004 \pm 0.002

Discussions

The network uncertainty can be estimated by randomly weakening node connections in a neural network. Randomly weakening these links will generate stochastic fluctuations and information loss when information passes through the information processing workflow passage defined by the neural network. The stochastic information loss can be used to measure the network

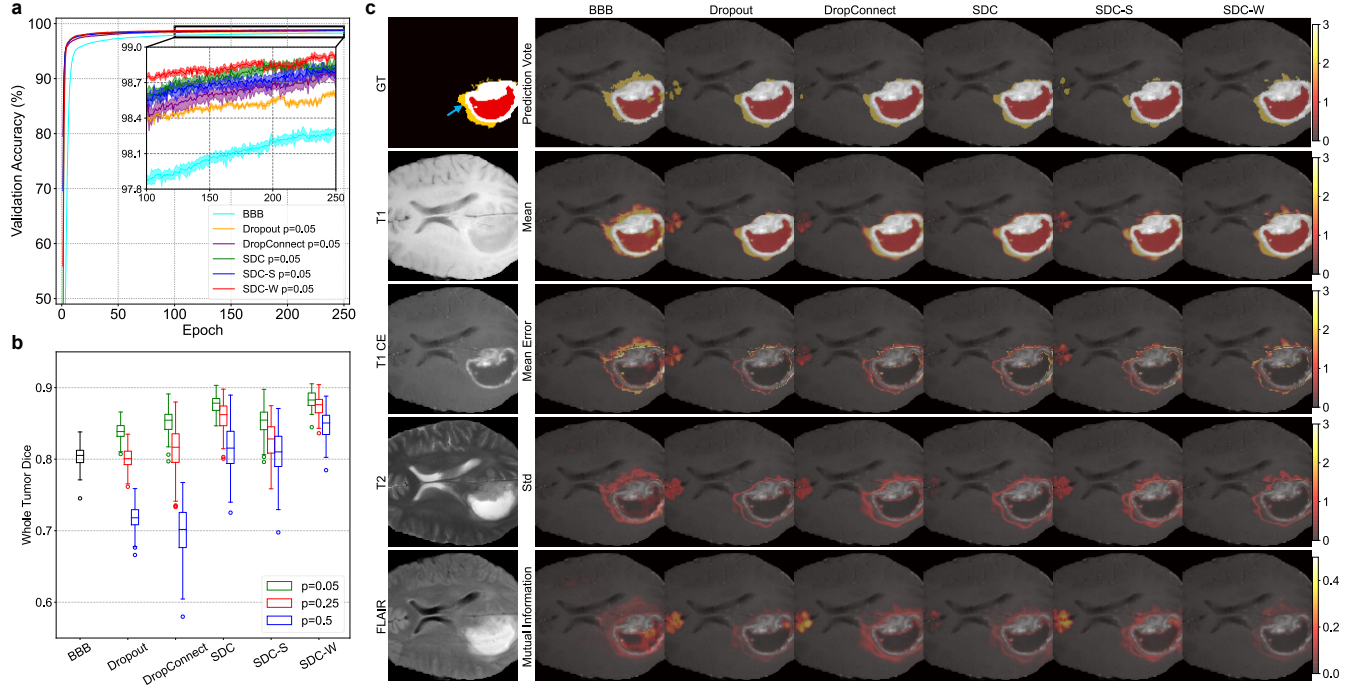


Figure 3. Uncertainty estimation results on the BraST dataset for gliomas segmentation. a) the validation accuracy in the training process with solid lines for average accuracy and bands for accuracy min-max range, b) the box plot of the whole tumor dice score on test data using different variational Bayesian inference methods with the leave out rate $p = 0.05, 0.25$ or 0.5 respectively, and c) a testing example of segmentation uncertainty with the leave out rate $p = 0.05$. In c), the left column shows ground truth and four MRI modalities. In the right part, each column shows prediction results using one method. The first row shows pixel-wise most popular votes. The second to fourth rows demonstrate pixel-wise average prediction, absolute error between ground truth and average predictions, and standard deviation respectively. The bottom row shows pixel-wise mutual information.

uncertainty. Suppose that there is a trained network which is very confident about its predictions, there must be sufficient information for the network to make predictions. Then, randomly leaving out a part of links would not change the network predictions dramatically because the network can utilize information redundancy to achieve performance robustness. On the other hand, for an unreliable network to make its predictions, the workflow would be much more fragile with respect to random connection dropouts, which should more likely change the predictions.

In this study, we have compared the six variational Bayesian inference methods, including our proposed SDC method and its two variants, on uncertainty estimation. Our experiments have been conducted for three tasks: one computer vision task for digit recognition, and two medical tasks for gliomas segmentation and metastases origin site classification respectively. Compared with the BBB, Dropout, and DropConnect methods, the proposed SDC method outperforms the others on all the three tasks, with higher accuracy and dice score as well as lower network uncertainty. Instead of directly discarding some connections of a node (DropConnect) or all connections of a node (Dropout), the proposed SDC method keeps node connects in principle while weakening them to different degrees by multiplying a random continuous variable such as $z^{ij} \sim U(0, 1)$. Such a design keeps an integrity of the information flow within the network so that there is less information loss than Dropout and DropConnect. Consequently, at the Monte Carlo inference stage SDC would lead to less information loss, resulting in less network uncertainty.

Based on our generic SDC design, we have further modified it into two variants by limiting the range of multiplicative weight modulation factors to form SDC-S and SDC-W schemes. Compared to the generic SDC, weight modulation factors in SDC-S are smaller, indicating node connections are weakened more severely. On the other hand, weight modulation factors in SDC-W are closer to 1 so that more information are kept. As shown in Fig. 2-4, SDC-W shows less uncertainty than SDC and SDC-S, which is an interesting phenomenon and consistent to our insight behind the SDC approach (an analogy is that soft thresholding is better than hard thresholding).

We have also investigated the effect of the leave out rate p on the network uncertainty. With the increment of p , more node connections are compromised, and there is more information loss in the information processing workflow, resulting in higher

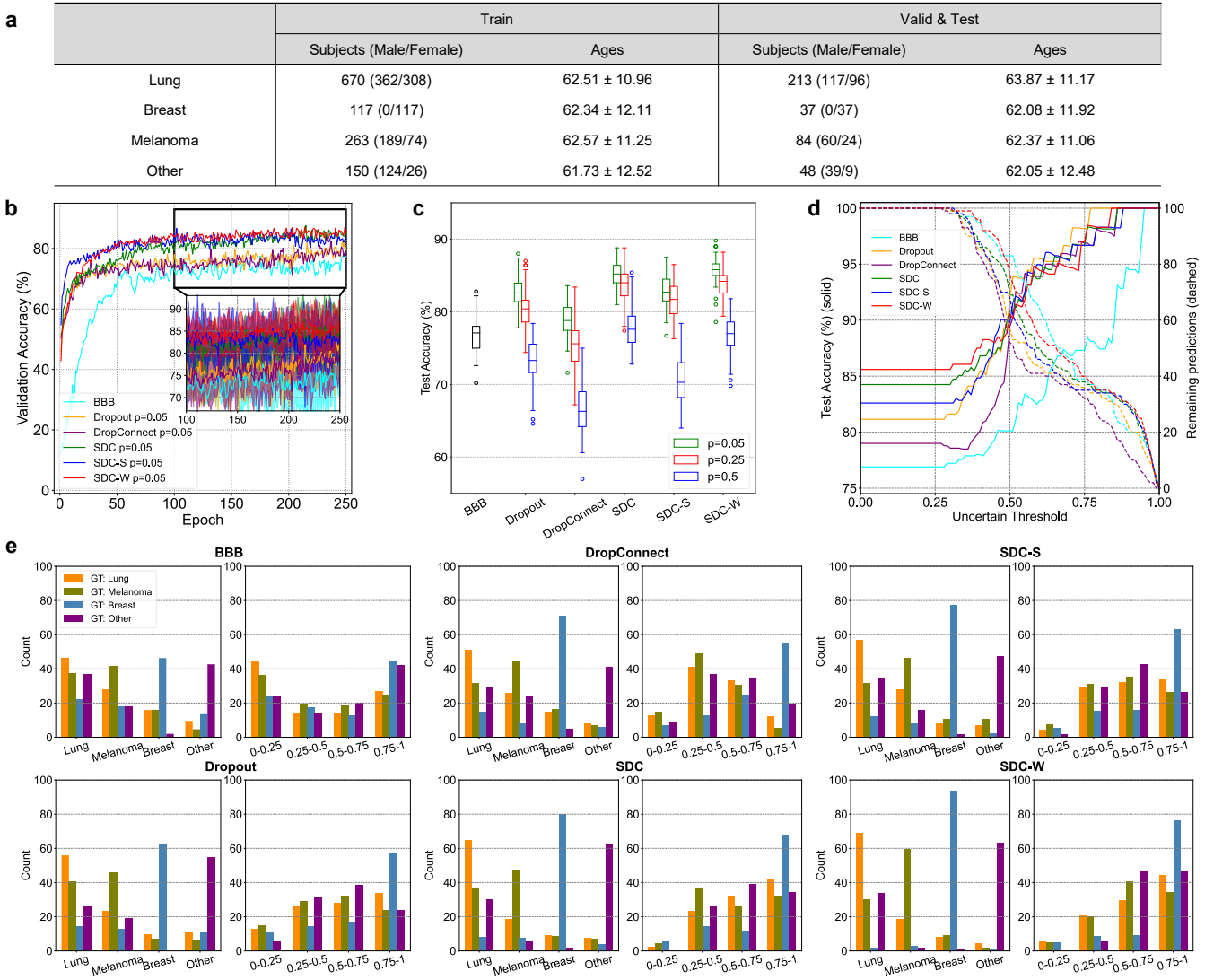


Figure 4. Uncertainty estimation results on the brain metastases dataset for tumor origin site classification. a) The dataset statistics, b) The validation accuracy in the training process with the solid lines for average accuracy and bands for accuracy min-max range, c) the box plot of whole tumor dice score on test data obtained using different variational Bayesian inference methods with $p = 0.05, 0.25$ and 0.5 respectively, d) the double y-axis plot showing curves of prediction accuracy and curves of remaining predictions with respect to the uncertain threshold with $p = 0.05$, and e) tumor origin site classification uncertainty testing results with $p = 0.05$. In each case, the left subplot shows average each class prediction counts, and the right subplot shows average softmax possibility counts of prediction popular voting class.

network uncertainty. Among the six methods compared in this study, SDC-W is the least affected one by the change of p , since there is generally the least information loss with SDC-W.

Network uncertainty estimation is not only useful but also necessary in medical applications. For segmentation tasks, as shown in Fig. 3d, areas with high uncertainty measured by standard deviation or mutual information are highly correlated with areas of false predictions. As a result, in real-world applications, radiologists should pay more attention to regions of high uncertainty, which helps mitigate false predictions. For classification tasks, Fig. 4c shows that higher prediction accuracy can be achieved by setting an appropriate uncertainty threshold to leave out some unreliable predictions. For those leave-out predictions, clinicians can perform classification aided by other methods such as biopsy³³ and bio-markers³⁴. Consequently, in reference to the network uncertainty, false predictions can be greatly alleviated. Clearly, this study shows a great potential of our SDC approach for network uncertainty estimation in future diagnosis and treatment planning, and improvement of healthcare outcomes and quality of life.

Methods

In this section, we first introduce variational Bayesian inference. Then, we describe neural network structures and experimental designs for all the three tasks performed in this study. Finally, we explain the key metrics used for evaluation of the competing network uncertainty methods.

Variational Bayesian inference

Bayesian neural network

Importantly, an artificial neural network can be viewed as a probabilistic model $p(y|x, w)$, where x , y , and w are input, output, and weight parameters respectively. In 2015, Blundell et al.¹⁷ performed an excellent study on weight uncertainty in neural networks. Here we briefly describe their approach using their notations. The parameters of a neural network as a probabilistic model can be optimized via maximum likelihood estimation (MLE) from a training dataset $D = (x_i, y_i)_i$ using a back-propagation algorithm.

$$\begin{aligned} w &= \arg \max_w p(D|w) \\ &= \arg \max_w \sum_i \log p(y_i|x_i, w). \end{aligned} \quad (1)$$

A more sophisticated way to optimize the probabilistic neural network is called maximum a posterior (MAP), when a parameter prior $p(w)$ is available. In this case, we have

$$\begin{aligned} w &= \arg \max_w p(w|D) \\ &= \arg \max_w \log p(D|w) + \log p(w). \end{aligned} \quad (2)$$

In the above formulation, the first and second terms reflect the data fidelity and the model complexity respectively.

Based on the parametric prior, a Bayesian neural network (BNN) seeks the posterior distribution of parameters $p(w|D)$, and performs its inference $p(y|x) = \mathbb{E}_{p(w|D)}[p(y|x, w)]$. After being trained, BNN parameters are in terms of possibility distributions, instead of point estimates as in the case of deterministic networks. As a result, network outputs and associated uncertainties can be naturally estimated. The parameter posterior distribution is computed based on the Bayes theorem:

$$p(w|D) = \frac{p(w, D)}{p(D)} = \frac{p(D|w)p(w)}{p(D)}, \quad (3)$$

where $p(D|w)$ and $p(D)$ are the likelihood function and the probability of the data. As (3) is intractable, variational inference is introduced to solve the problem. The key idea behind variational inference^{17,26,35} is to use a family of variational distributions $q(w|\theta)$ defined by the parameter θ to approximate the target posterior $p(w|D)$. For example, using a set of Gaussian distributions $\theta \sim N(\mu, \delta^2)$ as a surrogate of $p(w|D)$. The discrepancy should be minimized in terms of the Kullback-Leibler (KL) distance between $p(w|D)$ and $q(w|\theta)$:

$$\begin{aligned} \theta^* &= \arg \min_{\theta} D_{KL}[q(w|\theta) \| p(w|D)] \\ &= \arg \min_{\theta} \int q(w|\theta) \log \frac{q(w|\theta)}{p(w)p(D|w)} dw \\ &= \arg \min_{\theta} D_{KL}[q(w|\theta) \| p(w)] - \mathbb{E}_{q(w|\theta)}[\log p(D|w)]. \end{aligned} \quad (4)$$

Thus, the objective function can be expressed as follows:

$$\mathcal{F}(D, \theta) = D_{KL}[q(w|\theta) \| p(w)] - \mathbb{E}_{q(w|\theta)}[\log p(D|w)]. \quad (5)$$

To solve (5), Blundell et al.¹⁷ proposed Bayes by Backprop method via Monte Carlo sampling:

$$\mathcal{F}(D, \theta) \approx \sum_{i=1}^n \log q(w^{(i)}|\theta) - \log p(w^{(i)}) - \log p(D|w^{(i)}), \quad (6)$$

where $q(w^{(i)}|\theta)$ denotes the i^{th} Monte Carlo sample drawn from the variational distribution $q(w|\theta)$, and $w^{(i)}$ stands for the i^{th} Monte Carlo sample drawn from the prior distribution $p(w)$. In the training process, the mini-batch gradient descent is computed of

$$\mathcal{F}_i(D_i, \theta) = \frac{1}{M} D_{KL}[q(w|\theta) \| p(w)] - \mathbb{E}_{q(w|\theta)}[\log p(D_i|w)]. \quad (7)$$

where $\sum_i \mathcal{F}_i(D_i, \theta) = \mathcal{F}(D, \theta)$. The dataset is supposed to be uniformly and randomly divided into M minibatches. To solve (7), Blundell et al.¹⁷ introduced several techniques including unbiased Monte Carlo gradient computation, Gaussian variational posterior, scale mixture prior, KL re-weighting, and Thompson sampling. In this study, we implemented BBB based on³⁶.

SoftDropConnect (SDC)

It is challenging to implement traditional BNNs of complex structures¹¹. Alternatively, Gal et al. showed that Monte Carlo Dropout can be used to perform variational inference¹⁶. Compared with traditional BNNs, Dropout introduces no additional parameters and can be trained much faster. Additionally, Dropout can also work well with networks of complex structures. Furthermore, Mobiny et al. demonstrated that Monte Carlo DropConnect, replacing Dropout with DropConnect, to approximate Bayesian inference¹¹. It is found that DropConnect extracts uncertainty more robustly⁴. In another study, Dropout and DropConnect was cobmimed to produce even higher prediction accuracy with better robustness³⁷.

As originally proposed by Wan et al.³⁸, DropConnect is a generalization of Dropout³⁹ and is used to regularize neural networks. As shown in Fig. 1, for a fully-connect layers with M input nodes and N output nodes, DropConnect can be formulated as

$$v_{out} = \frac{\sigma[z \odot (w \cdot v_{in})]}{1 - p}, \quad (8)$$

where $v_{out} \in \mathbb{N}^{batch \times M}$ and $v_{in} \in \mathbb{N}^{batch \times N}$ are output and input vectors, respectively, p denotes the drop or leave out rate, $w \in \mathbb{N}^{M \times N}$ is the weight matrix, $z \in \mathbb{N}^{M \times N}$ is the drop weight matrix, \odot and σ signify the Hadamard product and activation respectively. In this work, we propose a method to change the drop matrix defined by a Bernoulli distribution $z^{ij} \sim Bernoulli(p)$ to the counterpart defined by a continuous uniform distribution $z^{ij} \sim U(0, 1)$. Compared with the original DropConnect that connections between nodes in adjacent layers are either kept or totally dropped, our proposed method is gentle, only weakening the connections by multiplying a continuous random weight modulation factor; for example, drawn from a uniform distribution between 0 and 1. To highlight this flexibility, we call our proposed method SoftDropConnect (SDC).

Based on the generic SDC design, we further specialize the SDC into two interesting variants SDC-S and SDC-W by limiting the random distribution to ranges of interest. Specifically, for SDC-S, $z^{ij} \sim U(0, 0.5)$, which weakens connections more strongly than SDC. For SDC-W, $z^{ij} \sim U(0.5, 1)$, which modulates network weights more gentle than SDC.

Neural networks

In each of our selected three tasks, the six variational Bayesian inference methods (BBB, Dropout, DropConnect, SDC, SDC-S, and SDC-W) were used in this study, which have the same network structure design.

MNIST digit recognition

Our network consists of two convolutional blocks followed by two fully-connected layers. Each convolutional block includes two convolutional layers followed by a batch normalization layer and a rectified linear unit (ReLU). Two max-pooling layers (kernel size of 2 and stride of 2) are after each convolutional block. Every convolutional layer has a kernel size of 3, stride of 1, and padding of 1. Totally, 32, and 64 kernels are used for the two convolutional blocks respectively. The first fully-connected layer has 3,136 input nodes and 1,024 output nodes, while the second fully-connected layer has 1,024 input nodes and 10 output nodes.

BraTS gliomas segmentation

We used the V-Net⁴⁰ for gliomas segmentation. There are 4 down-sampling blocks, a bottleneck block, 4 up-sampling blocks, and a final 3D convolutional layer. In each down-sampling block, there are two 3D convolutional layers. Each convolutional layer is followed by a batch normalization layer and a ReLU layer. 3D max-pooling layers are after each down-sampling block with kernel size of 2 and stride of 2. The number of kernels in down-sampling blocks are 16, 32, 64 and 128 respectively. The bottleneck block has two 3D convolutional layers with 256 kernels followed by batch normalization and ReLU activation. Each up-sampling block has an up-sampling layer with a factor of 2, and three 3D convolutional layers followed by batch normalization and ReLU activation. The number of kernels in the up-sampling blocks are 128, 64, 32 and 16 respectively. Skip connections link the output of the down-sampling blocks and the second convolutional layer in the up-sampling blocks. All the convolutional layers are with a kernel size of 3, stride of 1, and padding of 1.

Brain metastases origin site classification

We modified the tumor classification network used in our previous work³¹ to work on a single GPU. There are two identical feature extraction modules, an attention module, and a fully-connected modules. Compared with the original network, we modified the feature extraction module and the attention module. In the attention module, we changed the number of channel attention convolutional kernels from 512 to 256. In each feature extraction module, there are an initial 3D convolutional layer with 16 kernels and five convolutional blocks with 16, 32, 64, 128 and 256 kernels respectively. Each convolutional block has two identical 3D convolutional layers followed by batch normalization and ReLU activation. There is a 3D maxpooling layer with the kernel size of (1,2,2) and stride of (1,2,2) before the second and fourth convolutional blocks. Before the first, third, and fifth convolutional blocks respectively, there is a 3D maxpooling layer with kernel size of (2,2,2) and stride of (2,2,2). All convolutional layers are with a kernel size of 3, stride of 1, and padding of 1.

Implementation details

For the MNIST digit recognition task, the training process continued for 500 epochs with a learning rate of 0.001 and a batch size of 64. For the BBB method, each image was repeatedly input into the network five times before the gradient back propagation, and other methods only input each image once. For all the methods, each inference was based on repeatedly inputting an image into the network 25 times in each validation step, and 100 times in each testing step. Cross-entropy was used in the objective function.

When performing the BraTS gliomas segmentation, we set the total number of epochs to 250, a learning rate of 0.001, and a batch size of 2. For the BBB method, different from the MNIST digital classification, the number of input repetitions was 3 instead of 5 in each training gradient back propagation step. At the validation and testing stages, for all the methods each case was repeatedly inferred 10 times and 100 times, respectively. The summation of dice score and cross-entropy served as the objective function.

Similar to the design for gliomas segmentation, the training process for brain metastases tumor origin site classification continued for 250 epochs with a batch size of 2. The learning rate was set to 0.0001. Each case was repeated input to the network 3 times during the BBB training. For all the methods, the protocols for validation and testing were the same as that for gliomas segmentation. For this task, we adopted the weighted cross-entropy as the objective function.

In all the experiment, the Adadelta optimizer⁴¹ was used with a rho of 0.9, eps of 1e-06, and no weight decay. In each epoch, we recorded mean validation accuracy, as shown in Fig. 2a, 3b, and 4a. All the experiments were conducted in PyTorch 1.6.0 on a single NVIDIA Tesla V100 GPU with 32GB memory.

Network uncertainty metrics

Mutual information (MI) is widely used for measuring epistemic uncertainty for classification tasks. MI measures the expected divergence between the stochastic softmax output and the expected softmax output⁴. The expected softmax output can be calculated using as follows:

$$\hat{p} = \mathbb{E}_{\theta \sim p(\theta|D)}[p(y|x, \theta)]. \quad (9)$$

MI uses the entropy to measure the mutual dependence between two variables:

$$MI(\theta, y|x, D) = H[\hat{p}] - \mathbb{E}_{\theta \sim p(\theta|D)}H[p(y|x, \theta)], \quad (10)$$

where H is the entropy

$$H(p) = - \sum_{k=1}^K p_k \log_2(p_k). \quad (11)$$

In all our three tasks, two of them are for classification, and the other is for segmentation. As segmentation can be seen as pixel-wise classification, we adopted MI to measure epistemic uncertainty in all three tasks.

Additionally, we selected more metrics to measure network uncertainty. Standard deviation was used to measure the dispersion of network outputs. A lower standard deviation shows a better consistency of network outputs, indicating lower network uncertainty. Moreover, we analyzed the statistics of the network outputs and the last layer softmax possibility values to reveal the network uncertainty.

References

1. Gu, Y. *et al.* Automatic lung nodule detection using a 3D deep convolutional neural network combined with a multi-scale prediction strategy in chest CTs. *Comput. biology medicine* **103**, 220–231 (2018).
2. Isensee, F., Jäger, P. F., Full, P. M., Vollmuth, P. & Maier-Hein, K. H. nnU-Net for brain tumor segmentation. In *International MICCAI Brainlesion Workshop*, 118–132 (Springer, 2020).
3. Munir, K., Elahi, H., Ayub, A., Frezza, F. & Rizzi, A. Cancer diagnosis using deep learning: a bibliographic review. *Cancers* **11**, 1235 (2019).
4. Gawlikowski, J. *et al.* A survey of uncertainty in deep neural networks. *arXiv preprint arXiv:2107.03342* (2021).
5. Leynes, A. P. *et al.* Attenuation coefficient estimation for PET/MRI with bayesian deep learning pseudo-ct and maximum likelihood estimation of activity and attenuation. *arXiv preprint arXiv:2001.03414* (2020).
6. Ballestar, L. M. & Vilaplana, V. Mri brain tumor segmentation and uncertainty estimation using 3D-UNet architectures. *arXiv preprint arXiv:2012.15294* (2020).
7. Hepp, T. *et al.* Uncertainty estimation and explainability in deep learning-based age estimation of the human brain: Results from the German National Cohort MRI study. *Comput. Med. Imaging Graph.* **92**, 101967 (2021).
8. Tanno, R. *et al.* Uncertainty modelling in deep learning for safer neuroimage enhancement: Demonstration in diffusion MRI. *NeuroImage* **225**, 117366 (2021).
9. Narnhofer, D. *et al.* Bayesian uncertainty estimation of learned variational MRI reconstruction. *arXiv preprint arXiv:2102.06665* (2021).
10. Kendall, A. & Gal, Y. What uncertainties do we need in bayesian deep learning for computer vision? *arXiv preprint arXiv:1703.04977* (2017).
11. Mobiny, A. *et al.* DropConnect is effective in modeling uncertainty of bayesian deep networks. *Sci. reports* **11**, 1–14 (2021).
12. Gal, Y. *Uncertainty in deep learning*. Ph.D. thesis, University of Cambridge (2016).
13. Sensoy, M., Kaplan, L. & Kandemir, M. Evidential deep learning to quantify classification uncertainty. *arXiv preprint arXiv:1806.01768* (2018).
14. Malinin, A. & Gales, M. Predictive uncertainty estimation via prior networks. *arXiv preprint arXiv:1802.10501* (2018).
15. Raghu, M. *et al.* Direct uncertainty prediction for medical second opinions. In *International Conference on Machine Learning*, 5281–5290 (PMLR, 2019).
16. Gal, Y. & Ghahramani, Z. Dropout as a bayesian approximation: Representing model uncertainty in deep learning. In *international conference on machine learning*, 1050–1059 (PMLR, 2016).
17. Blundell, C., Cornebise, J., Kavukcuoglu, K. & Wierstra, D. Weight uncertainty in neural network. In *International Conference on Machine Learning*, 1613–1622 (PMLR, 2015).
18. Lakshminarayanan, B., Pritzel, A. & Blundell, C. Simple and scalable predictive uncertainty estimation using deep ensembles. *arXiv preprint arXiv:1612.01474* (2016).
19. Valdenegro-Toro, M. Deep sub-ensembles for fast uncertainty estimation in image classification. *arXiv preprint arXiv:1910.08168* (2019).
20. Wen, Y., Tran, D. & Ba, J. Batchensemble: an alternative approach to efficient ensemble and lifelong learning. *arXiv preprint arXiv:2002.06715* (2020).
21. Shorten, C. & Khoshgoftaar, T. M. A survey on image data augmentation for deep learning. *J. Big Data* **6**, 1–48 (2019).
22. Wen, Q. *et al.* Time series data augmentation for deep learning: A survey. *arXiv preprint arXiv:2002.12478* (2020).

23. Wang, G., Li, W., Ourselin, S. & Vercauteren, T. Automatic brain tumor segmentation using convolutional neural networks with test-time augmentation. In *International MICCAI Brainlesion Workshop*, 61–72 (Springer, 2018).
24. Wang, G. *et al.* Aleatoric uncertainty estimation with test-time augmentation for medical image segmentation with convolutional neural networks. *Neurocomputing* **338**, 34–45 (2019).
25. Neal, R. M. *Bayesian learning for neural networks*, vol. 118 (Springer Science & Business Media, 2012).
26. Graves, A. Practical variational inference for neural networks. *Adv. neural information processing systems* **24** (2011).
27. Kingma, D. P., Salimans, T. & Welling, M. Variational dropout and the local reparameterization trick. *Adv. neural information processing systems* **28**, 2575–2583 (2015).
28. Louizos, C. & Welling, M. Multiplicative normalizing flows for variational bayesian neural networks. In *International Conference on Machine Learning*, 2218–2227 (PMLR, 2017).
29. LeCun, Y. The MNIST database of handwritten digits. <http://yann.lecun.com/exdb/mnist/> (1998).
30. Baid, U. *et al.* The RSNA-ASNR-MICCAI BraTS 2021 benchmark on brain tumor segmentation and radiogenomic classification. *arXiv preprint arXiv:2107.02314* (2021).
31. Lyu, Q. *et al.* A transformer-based deep learning approach for classifying brain metastases into primary organ sites using clinical whole brain MRI images. *arXiv preprint arXiv:2110.03588* (2021).
32. Smith, L. & Gal, Y. Understanding measures of uncertainty for adversarial example detection. *arXiv preprint arXiv:1803.08533* (2018).
33. Vaidyanathan, R., Soon, R. H., Zhang, P., Jiang, K. & Lim, C. T. Cancer diagnosis: from tumor to liquid biopsy and beyond. *Lab on a Chip* **19**, 11–34 (2019).
34. Wu, L. & Qu, X. Cancer biomarker detection: recent achievements and challenges. *Chem. Soc. Rev.* **44**, 2963–2997 (2015).
35. Gal, Y. & Ghahramani, Z. Bayesian convolutional neural networks with bernoulli approximate variational inference. *arXiv preprint arXiv:1506.02158* (2015).
36. Shridhar, K., Laumann, F. & Liwicki, M. A comprehensive guide to bayesian convolutional neural network with variational inference. *arXiv preprint arXiv:1901.02731* (2019).
37. McClure, P. & Kriegeskorte, N. Robustly representing uncertainty through sampling in deep neural networks. *arXiv preprint arXiv:1611.01639* (2016).
38. Wan, L., Zeiler, M., Zhang, S., Le Cun, Y. & Fergus, R. Regularization of neural networks using DropConnect. In *International conference on machine learning*, 1058–1066 (PMLR, 2013).
39. Srivastava, N., Hinton, G., Krizhevsky, A., Sutskever, I. & Salakhutdinov, R. Dropout: a simple way to prevent neural networks from overfitting. *The journal machine learning research* **15**, 1929–1958 (2014).
40. Milletari, F., Navab, N. & Ahmadi, S.-A. V-Net: Fully convolutional neural networks for volumetric medical image segmentation. In *2016 fourth international conference on 3D vision (3DV)*, 565–571 (IEEE, 2016).
41. Zeiler, M. D. Adadelta: an adaptive learning rate method. *arXiv preprint arXiv:1212.5701* (2012).

Acknowledgements

This work was partly supported by

Author contributions statement

All authors conceived the experiment(s), Q.L. conducted the experiment(s), Q.L and G.W. analysed the results. All authors reviewed the manuscript.

Code availability

We will publish codes after the acceptance of this paper.